"Traveling Solitary Wave Solutions in the Resonant Interaction of Equatorial Baroclinic and Barotropic Rossby Waves"

June 11, 2008

Undergraduate Thesis by: Amanda K. O'Rourke

Advisor: Joseph A. Biello

Department of Mathematics
University of California, Davis
1 Shields Ave.
Davis, CA 95616

Contents

Abstract

The exchange of energy between the tropical and extratropical atmosphere by means of synoptic scale wave interaction is of particular interest in understanding global teleconnection patterns. Recently, Majda and Biello (2003) derived a system of equations that describe the resonant interaction of baroclinic and barotropic Rossby wave trains over long time and space scales. Biello and Majda's (2004) discover of an analytic solitary wave motivates the current work in which we derive a fourth-order system of nonlinear ordinary differential equations by making a traveling wave ansatz and studying the resultant ODEs which describe the wave envelope in a moving reference frame. Solutions connect two fixed points in either homoclinic or heteroclinic orbits. To obtain these solutions, we study the resulting non-linear boundary value problem; either by treating the ratio of baroclinic/barotropic wave dispersions or by treating the location of the (minimum) fixed point as the eigenvalue. We classify solutions based on the number of nodes in the baroclinic and barotropic wave fields in addition to their rotational behavior in phase space. We find that the ratio of the number of nodes in the barotropic to that in the baroclinic eigenfunction is almost exactly proportional to the square root of the ratio of dispersions; a result which can be explained by a simple argument from linear theory. The wind fields of two heteroclinic solitary waves is shown to describe a propagating disturbance that demarcates the zonal boundary between two different equatorial climatologies.

1 Introduction

A fundamental question in geophysical fluid dynamics arises out of the complex interaction between the tropical and extratropical atmosphere: how do the tropics influence mid-latitude patterns on large spatial scales and two week time scales? One possible means of a tropical-extratropical teleconnection is through the interaction of synoptic scale atmospheric waves. Recently, Majda and Biello (2003) used asymptotic analysis to derive a set of partial differential equations that describe the resonant interaction of equatorial, zonally long (4500km) baroclinic and barotropic Rossby waves over time scales of one week to a month. In this thesis, we seek time independent traveling wave solutions to the Majda-Biello equations through the derivation of a fourth-order, nonlinear system of ordinary differential equations in the traveling reference frame. We can use these steady solutions to help identify and understand the underlying physical behavior of atmospheric wind patterns which exist in the tropics and extratropics. These equations are of further mathematical interest in that they are found to exhibit an infinite number of solitary wave solutions in the barotropic and baroclinic wave fields for varying background states.

In a strongly stratified, rotating fluid system such as the Earth's atmosphere, planetary scale waves can develop in the wind and pressure fields as a response to the change in the Coriolis parameter with latitude. These waves, known as Rossby waves, have a significant influence on both equatorial and midlatitude wave dynamics, including tropical monsoons, the Madden-Jullian Oscillaion, and El Niño. The interaction of waves in these two climatological regimes is of considerable interest in understanding global teleconnection patterns, particularly in how equatorially trapped baroclinic Rossby waves drive barotropic Rossby waves with a significant projection onto the midlatitudes. To determine the theoretical influence of localized, steady thermal forcing in the tropics on midlatitude dynamics, Webster (1972) and Kasahara and Silva Dias (1986) utilized a linearized two-layer global primitive equation model to find that the presence of mean horizontal and vertical shears in the tropics are necessary to generate a midlatitude response, thus suggesting that baroclinic Rossby waves can drive barotropic Rossby waves in the midlatitudes. However, the interaction between the tropics and midlatitudes is not unidirectional. Lin et al. (2000) showed that that midlatitude dynamics could trigger an intraseasonal tropical response using an intermediate climate model with baroclinic and barotropic vertical modes. In the study of Rossby waves in the large scale patterns of tropical and midlatitude atmosphere, Wang and Xie (1996) found coupling between the baroclinic and barotropic components of low-frequency Rossby waves in the presence of a vertically sheared background state in a two layer equatorial β-plane model.

The resonant interaction of nearly dispersionless Rossby waves, such as that

discussed by Wang and Xie (1996), permit the mutual exchange of energy between vertical modes. While baroclinic Rossby waves are confined near the equator, barotropic Rossby waves have significant projection onto higher latitudes, thus the resonant interaction of baroclinic and barotropic Rossby waves could provide a basis for the meridional exchange of energy between the tropics and midlatitudes.

Majda and Biello (2003) asymptotically derive a system of equations that describe the nonlinear interaction of planetary scale Rossby waves on an equatorial β-plane where x has been scaled for unforced, long zonal waves in the troposphere. These equations describe the evolution and interaction of coupled, unforced baroclinic and barotropic Rossby waves over long time scales. The canonical form of the Majda-Biello (MB) equations are

$$\begin{aligned} A_t - DA_{xxx} + BA_x + AB_x &= 0 \\ B_t - B_{xxx} + AA_x &= 0 \end{aligned} \tag{1}$$

where A and B are the amplitudes of the baroclinic and the barotropic wave fields, respectively, and are measured in wind speeds on the order of 5m/s. These equations are scaled about a zonal length of 4500km and a time of ten days. The ratio of dispersions between the waves, D, is a function of the meridional index, m and is found to be 0.889 and 0.96 for the first two meridional indices. Majda and Biello (2003) indicate that the first and second, $m = 1, 2$, equatorial baroclinic Rossby waves have significant interaction with off-equatorial barotropic Rossby waves. Waves with higher meridional indices, where $m \geq 3$, have an existing projection onto the midlatitudes, thus these baroclinic waves do not have as significant a contribution to a tropical-midlatitude teleconnection.

The similarity of the MB equations, (1), to the Korteweg-de Vries equation, through the dispersion and coupled, quadratic nonlinear terms, led Biello and Majda (2004) to an analytical solitary wave solution. The solitary wave takes the form of a squared hyperbolic secant that travels at a constant speed. The existence of this solitary wave motivates the current investigation into the existence of additional solitary waves in a traveling reference frame.

The present paper expands on the work of Majda and Biello (2003, 2004) through the introduction of a traveling reference frame to equations (1). In Section 2 we discuss the transformation of reference frames and the derivation of the traveling wave equations, including the influence of the conservation of energy on solutions of the system. The conserved quantity produces a potential well in phase space within which stable solutions exist. The numerical methods we use are described in Section 3 while the solutions themselves are discussed in Section 4.

Section 4.1 includes a brief overview of the initial value problem to the traveling wave system. In the initial value problem, solutions are found to group together

near a particular solution that connects a fixed point to itself in a homoclinic orbit: a solitary wave. This homoclinic solitary wave has similar structure to the analytic solitary wave found by Biello and Majda (2004).

Motivated by the possibility of further solitary wave solutions, we solve a nonlinear boundary value problem in Section 4.2 for solutions on the interval $[0, \infty]$, where the undetermined ratio of dispersions, D, is the eigenvalue. We are able to find both the homoclinic solitary waves suggested by the initial value problem as well as heteroclinic solitary waves for a range of ratios of dispersions. The physical profile of the heteroclinic wave is a localized, transitional disturbance between two climatological distinct wind regimes. Homoclinic solitary waves present as localized anomalies in the background flow that, unlike heteroclinic solitary waves, do not change the mean climatological profile of the tropical and midlatitude atmosphere.

In Section 4.2 we index the solitary waves by the number of nodes in the baroclinic and barotropic wave amplitudes. While this ordering allows us to distinguish each individual solitary waves, it can also be linked to the linear frequencies of these high energy oscillations and the ratio of dispersion, D. We discuss this relationship between the ratio of dispersions and the solitary wave index in Section 4.4.

The solitary waves we identify have been nondimensionalized against the characteristic length and time scales of baroclinic and barotropic Rossby waves. In Section 5.1 we reintroduce dimensionality to the baroclinic and barotropic wave fields and project them onto a latitude-longitude map to visualize the resulting wind field of selected solitary waves. We then analyze the resonant interaction of the equatorial baroclinic and barotropic Rossby wave modes for solitary wave cases in Section 5.2 through a discussion of the mathematical properties and physical relevance of both the $m = 1, 2$ meridional mode wind fields.

2 Traveling Wave Substitution and Energy

Through its similarity to the Korteweg-de Vries equation, Biello and Majda (2004) discover an analytical solitary wave solution to (1) in the form $\alpha \operatorname{sech}^2(\frac{x-ct}{\lambda}) - \gamma$ for constants α, λ, and γ. These solutions travel along characteristics of the system, $x - ct$, for a given speed c. We thus introduce a change of variables $\xi = x - ct$ to view the solutions to (1) in a traveling reference frame. Upon integrating the (1) once in ξ, we obtain a fourth order system of nonlinear ordinary differential equations

$$\begin{aligned} DA'' &= AB - cA - a \\ B'' &= \frac{A^2}{2} - cB - b. \end{aligned} \tag{2}$$

As before, A and B are the baroclinic and barotropic wind fields, respectively. The system contains three arbitrary constants: the wave speed, c, and two constants of integration, a and b, relating to the values of A and B as $\xi \to \pm\infty$. We note that, due to the structure of (2), we are restricted to positive wave speeds in order for the system to support oscillatory solutions near a fixed point. As the traveling wave system is derived from the original MB equations, (1), the analytic solitary wave solution found by Biello and Majda (2004) is also a solution to equations (2). The constants of integration, a and b determine location of the fixed points of the system and the behavior of solitary wave solutions as $\xi \to \pm\infty$.

The resonant interaction of the baroclinic and barotropic wave fields arises from the similarity in the dispersion relation of each Rossby wave packets. The ratio of dispersions, D, of the baroclinic and barotropic wave fields, as derived by Biello and Majda (2004), is the ratio of the baroclinic and barotropic dispersion relations and is a function of the baroclinic meridional wave index, m such that

$$D = 1 - \frac{1}{(2m+1)^2} \tag{3}$$

. We only consider the equatorially confined, low meridional index baroclinic waves in our approximation, thus the ratios of dispersions of interest for the first ($m = 1$) and second ($m = 2$) baroclinic wave fields are $D = 0.889$ and $D = 0.96$, respectively.

We can remove the traveling wave speed, c, from (2) by rescaling the traveling wave variable, ξ, the amplitudes of the baroclinic and barotropic wave fields, A and B, and the constants of the background flow, a and b. The traveling wave variable, ξ, is scaled by $\tilde{\xi} = c^{-\frac{1}{2}}\xi$. The baroclinic and barotropic wave fields can then be scaled as $\tilde{A} = cA$ and $\tilde{B} = cB$. Likewise, the constants which determine the background state of the system can be scaled as $\tilde{a} = c^2 a$ and $\tilde{b} = c^2 b$. After dropping the tildes, the system is equivalent to (2) with $c = 1$. Thus, without loss of generality, we consider only the $c = 1$ case.

The traveling wave system (2) contains a conserved quantity, the energy, so-called for its resemblance to standard physical energy equations with both a kinetic and potential term. The conservation of energy imposes a strong restriction on the dynamics and structure of the system. The energy, E, is a function of the wave fields, A and B, as well as their total derivatives and the constants a and b.

$$E = \frac{1}{2}(DA_x^2 + B_x^2 + A^2 + B^2 - A^2B) + aA + bB \tag{4}$$

Due to energy conservation, all solutions are restricted to a potential well in the A, B phase space.The potential energy is given by

$$V = \frac{1}{2}(A^2 + B^2 - A^2B) + aA + bB. \tag{5}$$

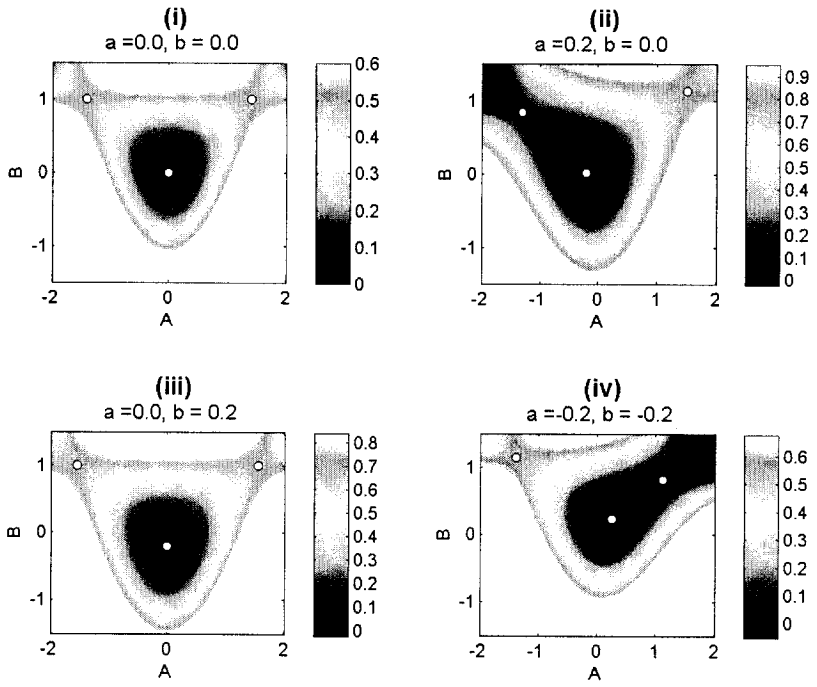

Figure 1: Four potential wells for varying values of a and b. White regions and regions of lower energy outside of the potential well are areas of unstable energy levels. Solutions at these energy levels are unbounded. For (i) and (iii), $a = 0$ and the potential well is symmetric and the saddle fixed points are at the same energy level. Changing a results in an asymmetry in the well, as shown in (ii) and (iv). The overall size and depth of the potential well can be adjusted by changing b; smaller b results in a smaller potential well.

The value of the constants a and b determine the location of the fixed points and the shape of the potential well. Potential wells for varying values of a and b are given in Figure 1. Solutions are bounded and finite only when there are three unique fixed points, two saddle points and a minimum in phase space, and when the energy level of a solution is less than the energy level of the saddle fixed points and greater than the energy level of the minimum fixed point. The maximum energy of all stable, bounded solutions is equal to the energy of the fixed saddle points. The location of the fixed points in (A, B) phase space are solutions to $\frac{\partial V}{\partial A} = 0$ and $\frac{\partial V}{\partial B} = 0$. Numerically, these points are the roots of a cubic in A.

$$\frac{1}{2}A^3 - (b+1)A - a = 0$$

with corresponding values of B

$$B = \frac{1}{2}A^2 - b.$$

Solitary wave solutions are known to connect either one saddle fixed point to itself in a homoclinic orbit or to connect the two individual saddle fixed points in a heteroclinic orbit. Heteroclinic solitary waves are of particular physical interest since they represent an organized, propagating disturbance that is identified by a sudden reversal of the upper and lower tropospheric climatology.

The existence of these heteroclinic solitary waves is dependent on the energy levels of the two saddle fixed points. By conservation of energy, both saddle points must be at the same energy level for a heteroclinic solitary wave to connect them and thus the energy difference between the two saddle points must be zero.

The energy level and location of the saddle points are a function of the constants a and b. Numerically, we consider the difference in energy between the two saddle points as a function of a and b on the contour plot in Figure 2.

We first note from Figure 2 that not all values of a and b result in two saddle points; the white regions indicate values of a and b for which there are no stable solutions to the traveling wave equation as the potential surface, (5), does not have a local minimum and thus does not produce a potential well. Two unique saddle points and stable solutions exist only when $b > \frac{3}{2}a^{\frac{2}{3}} - 1$. Additionally, the contour of zero energy difference is strictly located along the line $a = 0$. The location of the minimum and saddle fixed points are (A_{min}, B_{min}) and $(A_{\pm}, B_{\pm})$, respectively, and satisfy equations (6).

$$\begin{aligned} A_{min} = 0, \;\; B_{min} = -b \\ A_{\pm} = \pm\sqrt{2(b+1)}, \;\; B_{\pm} = 1 \end{aligned} \tag{6}$$

Heteroclinic solitary waves exist only for potential wells with saddle points located at equal energy levels and thus, as shown in Figure 2, only for potential

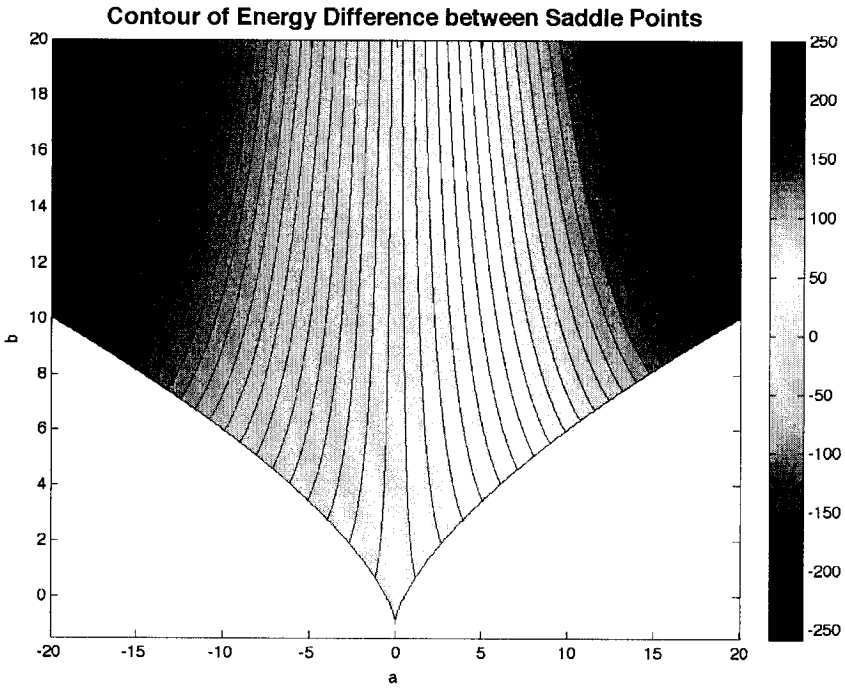

Figure 2: Contours of the difference in energy between the saddle points as a function of a and b. White areas indicate values of a and b that do not generate three unique fixed points and thus do not create a potential well.

wells where $a = 0$. Due to this, we focus our attention only on the case of $a = 0$ where we have a symmetric potential well, as seen in (i) and (iii) of Figure 1, with saddle fixed points located at $A_\pm$ and $B_\pm$ of (6).

3 Numerical Models

We initially explore the solution space of the traveling wave system, (2), using MATLAB's variable time-step Runga-Kutta numerical integrator for various initial values of A, B, A' and B'. Solutions are found for the basic case of $D = 1$, $a = 0$, and $b = 0$. We choose initial values for the baroclinic and barotropic wave fields at various energy levels within the potential well and classify solutions on their observed behavior in (A, B) phase space.

We then find solitary wave solutions using MATLAB's integrated boundary value solver with an unknown eigenvalue; either the ratio of dispersions, D, in Section 4.1, or barotropic constant of integration, b, in Section 4.2. We solve for solutions at infinity by continuously expanding the integration domain until we achieve a convergent eigenvalue and eigenfunction. In order to use MATLAB's boundary value problem solver, we utilize the symmetries present in both the heteroclinic and homoclinic solitary waves to split each solitary wave in half and find solutions over the domain of $[0, \infty]$. In both heteroclinic and homoclinic solitary waves, the barotropic wind field, B, is symmetric while the baroclinic wind field, A, is antisymmetric for heteroclinic solitary waves and symmetric for homoclinic solitary waves.

The boundary conditions for both homoclinic and heteroclinic solitary waves at infinity are the same; the values of A and B must exponentially decay into the fixed points at infinity and thus the derivatives, $A'(\pm\infty)$ and $B'(\pm\infty)$ must vanish. As the heteroclinic solitary waves are antisymmetric about $\xi = 0$ in the baroclinic wave field, $A(0)$ must vanish. Likewise, the homoclinic solitary waves are symmetric in both the barotropic and baroclinic wave field, thus the derivatives, A' and B', must vanish at $\xi = 0$. Although any five of these boundary conditions are sufficient, we choose to integrate using the four constraints at infinity and the restrictions on A and A' at $\xi = 0$, depending on the type of solitary wave we wish to identify.

For all numerical solutions, we are able to estimate the error through conservation of energy. For the initial value problem, integration tolerances are set to 10^{-10} while the boundary value problem solver has integration tolerances of 10^{-13}. The energy loss, or the difference in energy between the initial or boundary conditions and the intermediate time-steps, is on the order of 10^{-7} for the initial value problem and 10^{-9} for the boundary value problem solver.

4 Solutions to the Traveling Wave Equations

4.1 Initial Value Problem

We begin with an overview of the typical solutions to the initial value problem of equations (2). Due to the conservation of energy, our focus is on the structure of solutions in (A, B) phase space which we describe as orbits within the potential well. We begin with the simplest form of (2) by setting $D = 1$ and $a = b = 0$. By our choice of the ratio of dispersions, D, we add resonance between the baroclinic and barotropic wave amplitudes, A and B. The ratio of dispersions acts as a weight to the oscillations in A and B much like a mass would act as a weight on a spring. Oscillations in the barotropic wave amplitudes, B, are more frequent than oscillations in A for $D > 1$ and for $D < 1$, oscillations occur more often in the baroclinic wave amplitudes, A. By choosing $D = 1$, we force a resonance between the frequencies of baroclinic and barotropic wave fields such that each oscillate at approximately the same rate. This forced relationship between the oscillation frequency in A and in B results in a unique, straight-line orbit in phase space, a cnoidal wave, that hints at the existence of solitary waves.

The potential well for the initial value problem contains three fixed points: two saddle points and a minimum. As we have chosen $a = 0$, the potential well is symmetric in A and achieves its maximum energy at both of the saddle points. The saddle points are located at $(\pm\sqrt{2}, 1)$ in (A, B) and have an energy of $E = \frac{1}{2}$. The minimum fixed point is located at the origin at the zero energy level. The potential well is the same as that observed in (i) of Figure 1 and resembles a radially symmetric bowl near the origin. At higher energy levels, the bowl distorts such that the line of maximum energy lies along the line $B = 1$ and the parabola $B = A^2 - 1$.

Solutions to the initial value problem, as viewed in phase space, fall into two broad categories: ball orbits and solitary wave 'ghosts'. Ball orbits, such as those in Figure 3 are circular in shape and are symmetric in A. They do not approach either saddle fixed point and are, instead, confined to a the region around the minimum of the potential well. The behavior of $A(\xi)$ and $B(\xi)$ are found to have a unique 'bursting' behavior over a long time scale such that an initially energetic barotropic mode later excites an energetic baroclinic mode. These 'bursts' present as a slowly varying envelope containing rapid oscillations in both A and B and motivate a multi-scale asymptotic analysis around the local minimum. Although this analysis is beyond the scope of this paper, these ball orbits are found to limit to solitary waves on long time scales and have integrable solutions due to the derivation of an additional conserved quantity. The combination of this new conserved quantity and the energy, (4), effectively reduce the traveling wave system over long time scales from one of coupled, fourth-dimensional nonlinear equations

to a fully integrable, two dimensional system.

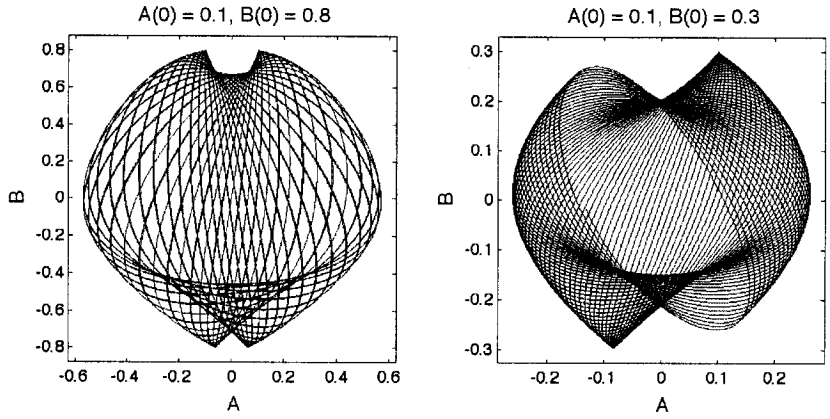

Figure 3: Ball orbits for initial values of $(0.1, 0.8)$ and $(0.1, 0.3)$. Initial derivatives of the wave field, A_x and B_x are both zero. Solutions fill the space around the origin and do not interact significantly with the saddle fixed points

While the ball orbits contain mathematically interesting 'bursting' solutions in the A and B wave fields, these solutions do not display true solitary wave solutions on the time scales of 2, such as those which connect saddle fixed points. Unlike ball orbits, solitary wave 'ghost' solutions, such as the two in Figure 4, stay within the region connecting the saddle fixed points of the system to the minimum. Solutions of this type appear to remain near certain preferred paths. In the case of the initial value problem with $D = 1$ and $a = b = 0$, these preferred paths are the lines connecting the origin to either of the two saddle fixed points at $(\pm\sqrt{2}, 1)$.

Motivated by the preference of these 'ghost' orbits, we choose initial conditions within an epsilon distance of the saddle fixed point, or at $(\pm\sqrt{2} - \epsilon, 1 - \epsilon)$. Due to small errors in the initial value problem solver and the high energy level of the saddle node fixed point, solutions starting directly on the fixed point will fall outside of the potential well and become unbounded. As shown in Figure 5, we find a cnoidal wave which connects one saddle fixed point to the origin in a straight line. In $A(\xi)$ and $B(\xi)$, these cnoidal waves resemble a chain of hyperbolic secant bursts.

The cnoidal wave orbit lies along this straight line path due to our choice of the ratio of dispersions. By setting $D = 1$, we have created a resonance between the amplitudes of the baroclinic and barotropic wave fields. We force equality in the weighting of oscillations in A and B, thus there is no preferred curvature to the orbit in either the A or B direction.

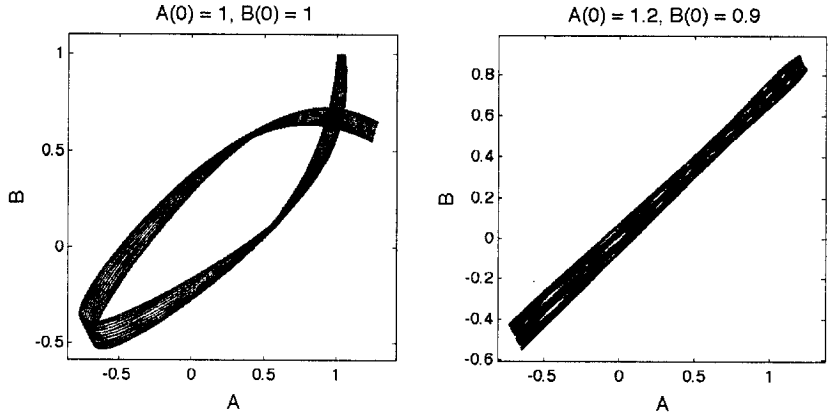

Figure 4: Solitary wave 'ghost' solutions to the initial value problem of the traveling wave system for the initial points $(1, 1)$ and $(1.2, .9)$. Initial A_x and B_x are both zero. Solutions are bounded within the region of the line connecting the minimum fixed point to either of the two saddle points. In this case, initial positions are chosen such that solutions oscillate between the $(\sqrt{2}, 1)$ saddle point and the origin.

4.2 Boundary Value Problem

The cnoidal wave in the initial value problem suggests the presence of a homoclinic solitary wave that connects a saddle point to itself. However, by fixing both the ratio of dispersions and the shape of the potential well, we are only able to identify one solitary wave. Instead, we allow one parameter to vary as an undetermined eigenvalue in a boundary value problem. The boundary value problem allows us to find not only the homoclinic orbits that connect one saddle fixed point to itself, but we also find heteroclinic orbits connect both saddle fixed points to each other.

Unlike homoclinic solitary waves, heteroclinic solitary waves require the existence of two unique saddle points. Additionally, both saddle points must be at the same energy level in order for a heteroclinic solitary wave to connect the fixed points. This occurs only for symmetric potential wells, or those with $a = 0$. As both homoclinic and heteroclinic orbits can exist for a symmetric potential well, we examine the solitary waves present in those potential wells with $a = 0$. We find unique solitary waves by allowing the ratio of dispersions, D or the shape of the potential well, b, to vary. Both cases, either with a fixed b or a fixed D, pose a boundary value problem with one undetermined eigenvalue.

We establish a means of uniquely classifying solitary waves by the number of nodes in the baroclinic and barotropic wave fields. Each solitary wave then represents an eigenmode with two indices, n_a and n_b for the number of times $A(\xi) = 0$ and $B(\xi) = 0$, respectively. The solitary wave from the initial value

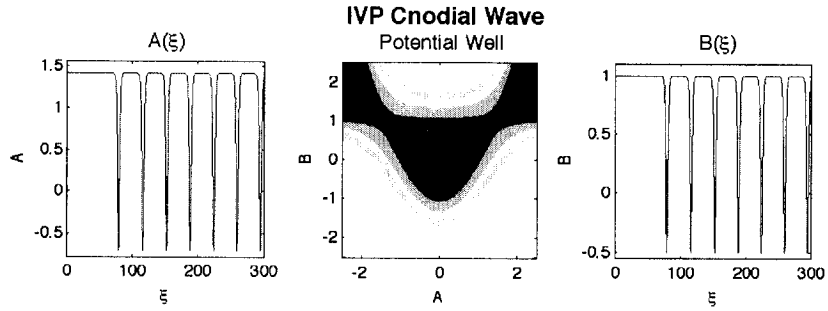

Figure 5: The cnoidal wave in the initial value problem with an initial condition of $(\sqrt{2}-\epsilon, 1-\epsilon)$ with $\epsilon = 10^{-16}$ and $A_x = B_x = 0$. The center graph is one of the orbit plotted against the potential well in phase space showing the straight-line connection between the minimum and saddle point. In $A(\xi)$ and $B(\xi)$ the solutions resembled connected hyberbolic secants after a brief initial, constant period.

problem, for example, would have $n_a = 2$ and $n_b = 2$ as it has two nodes in both the baroclinic and barotropic wind fields. As we are solving a eigenvalue problem, we label each eigenmode as n_a, n_b, thus the initial value problem solitary wave would be eigenmode $2, 2$.

We note that even indices are a result of the solitary wave returning to the same value of A or B as $\xi \to \pm\infty$. For all symmetric potential wells where $a = 0$, the saddle fixed point is always located along the line $B = 1$. Therefore all solitary wave orbits, regardless if they are heterocilnic or homoclinic, have a barotropic wave field that asymptotes to $B = 1$ at $\xi = \pm\infty$ and thus have an even n_b index. A similar argument holds for n_a in a homoclinic orbit as these solitary waves begin and end at the same fixed point, thus A approaches the same value as ξ goes to infinity. However, n_a is odd for heteroclinic orbits as the baroclinic wave field has different values at $A(-\infty)$ and $A(\infty)$.

In the A, B phase space, the ratio of dispersions acts to weigh the direction of the orbit along either A or B and acts as a frequency splitting parameter. For $D > 1$, the barotropic wave amplitude, B, contains more oscillations than that in the baroclinic wave field, A, resulting in an initial, upward curve to the orbit. For $D < 1$ the opposite is true; there are more oscillations in A than in B and the orbit will first curve towards negative B after exiting the saddle point. For $D = 1$, as was the case in the initial value problem, the ratio of oscillations in A and B are the same, resulting in the straight line solitary wave connecting the minimum to either of the two saddle points in the potential well. By changing D, we permit solutions exiting the fixed point to curve, a necessary condition for

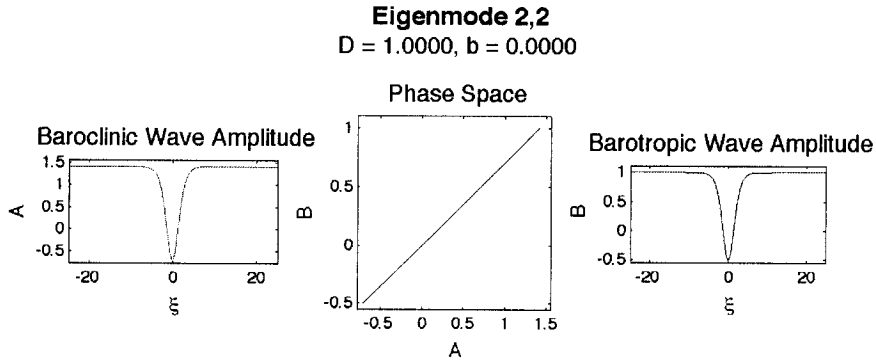

Figure 6: Eigenmode 2,2, the homoclinic solitary wave predicted from the initial value problem, for a fixed potential well.

connecting both fixed points in a heteroclinic solitary wave and for finding curved homoclinic orbits.

For the eigenvalue problem in D, we fix $b = 0$ to compare with the solutions found in the initial value problem. We find numerous solitary waves with D ranging from 0.06 to 3.2, including the solitary wave associated with the initial value problem's cnoidal wave at $D = 1$ (Figure 4.2).

Homoclinic solitary waves are found for ratios of dispersions both greater than and less than one, such as Eigenmodes 6,4 and 4,6 in Figures 7 and 8, respectively. These orbits are nearly mirrored reflections of each other across the line connecting the right-most saddle point with the origin. Similarly, we note that for $D > 1$ the orbit initially curves upward, indicating an unequal weighting between the baroclinic and barotropic wave fields that suppresses the oscillations in A as compared to B. The opposite is true for $D < 1$ where the orbits initially curve downward in B. The pattern of initial curvature and its dependence on D is also found in the heteroclinic orbits for a fixed potential well, such as in the case of Eigenmode 3,2 and 3,4 in Figures 9 and 10. This unequal weighting and relationship to the value of D with respect to 1 can be identified by the indexing. For $n_a > n_b$, we find that $D < 1$. Likewise, if $n_a < n_b$, $D > 1$.

In addition to the behavior of the orbit's initial curvature with respect to D, we note an additional behavior in the heteroclinic orbits. Certain heteroclinic solitary waves stand out for their simplicity and unidirectional rotation around the minimum of the potential well. These orbits, such as those in Figures 9 and 10, circle the origin in either a strict clockwise or counterclockwise direction, depending on the orbit's initial saddle point. For example, the Eigenmode 3,2 solitary wave enters the basin of the potential well from the leftmost saddle point and circles the

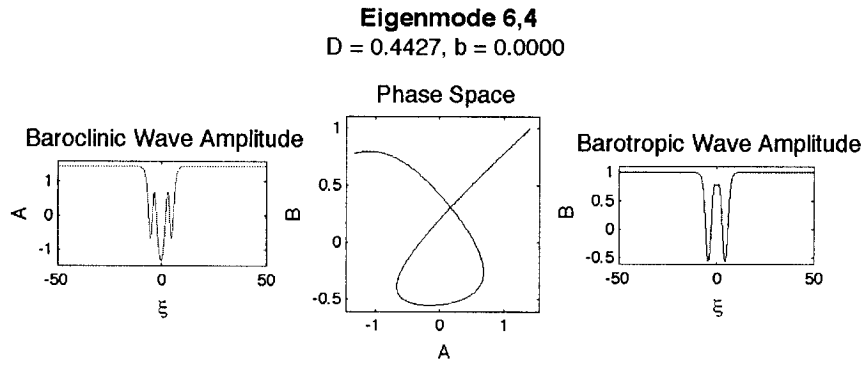

Figure 7: Eigenmode 6,4 with $D = 0.4427 < 1$ showing an initial downward curvature out of the fixed point in a homoclinic orbit.

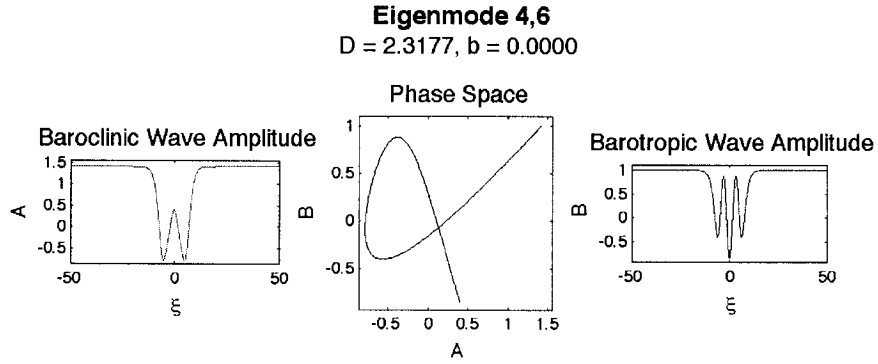

Figure 8: Eigenmode 4,6 with $D = 2.3177 > 1$ showing an initial upward curvature out of the fixed point in a homoclinic orbit.

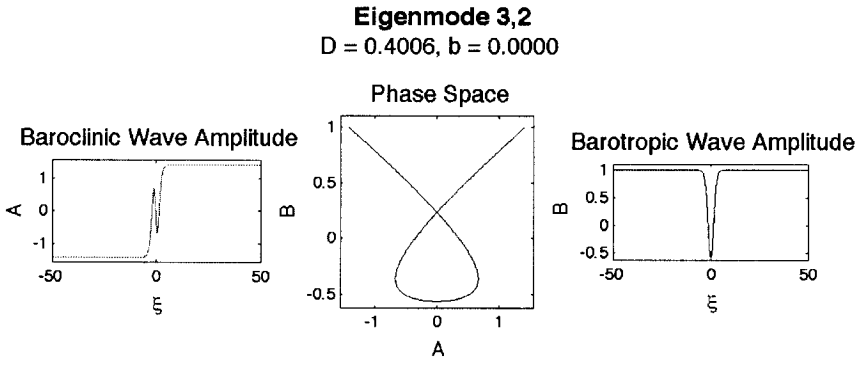

Figure 9: Eigenmode 3,2 with $D = 0.4006 < 1$ showing an initial downward curvature out of the fixed point in a heteroclinic orbit.

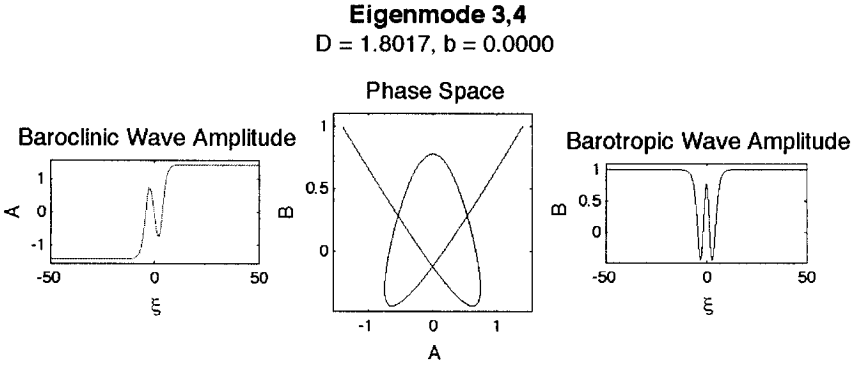

Figure 10: Eigenmode 3,4 with $D = 1.8017 > 1$ showing an initial upward curvature out of the fixed point in a heteroclinic orbit.

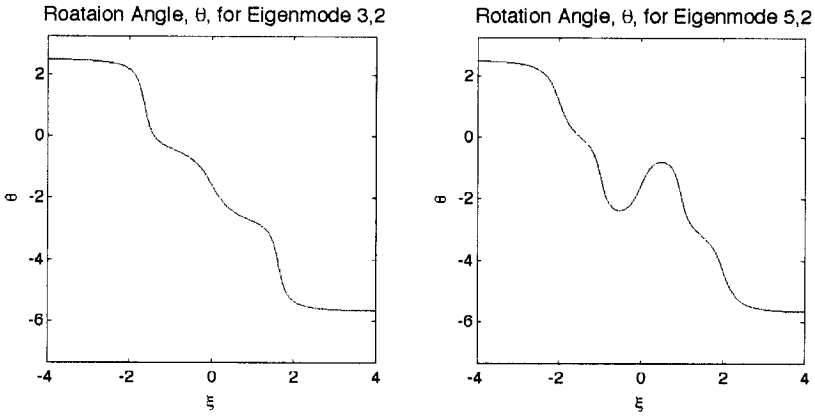

Figure 12: The heteroclinic, eigenmode 5,2 solitary wave reverses its rotation around the origin near the mid-point of its orbit. It the first overtone of the $n_a = 5$ solitary waves.

all fundamental solitary waves have the property that $n_a - n_b = 1$. The first four fundamental solitary waves in a fixed potential well are shown in the Appendix.

4.4 Indices and Linear Frequencies

Beyond the winding number, the nodal indices have a deeper connection the fundamental properties of the traveling wave system when we consider a linear approximation to (2) around the potential well minimum. The solitary wave solutions we have found have oscillations in the baroclinic and barotropic wave field which occur around the minimum fixed point. For all symmetric potential wells, the minimum fixed point lies along the line $A = 0$. The bulk of the solitary wave oscillations occur within an ϵ distance of the line $A = 0$, suggesting the nonlinear terms of (2) are small despite the high energy level of the solitary waves. By letting $A \rightarrow 0 + \tilde{A}$ and $B \rightarrow -b + \tilde{B}$, substituting into (2), and collecting the first order terms, we obtain:

$$\tilde{A}'' + \frac{b+1}{D}\tilde{A} = 0$$
$$\tilde{B}'' + \tilde{B} = 0$$

In this linearized approximation, the frequencies in A and B are approximately $\omega_A = \sqrt{\frac{b+1}{D}}$ and $\omega_B = 1$. The frequency of an oscillating solution is directly related to the number of nodes within a given period. The period, or the length of ξ

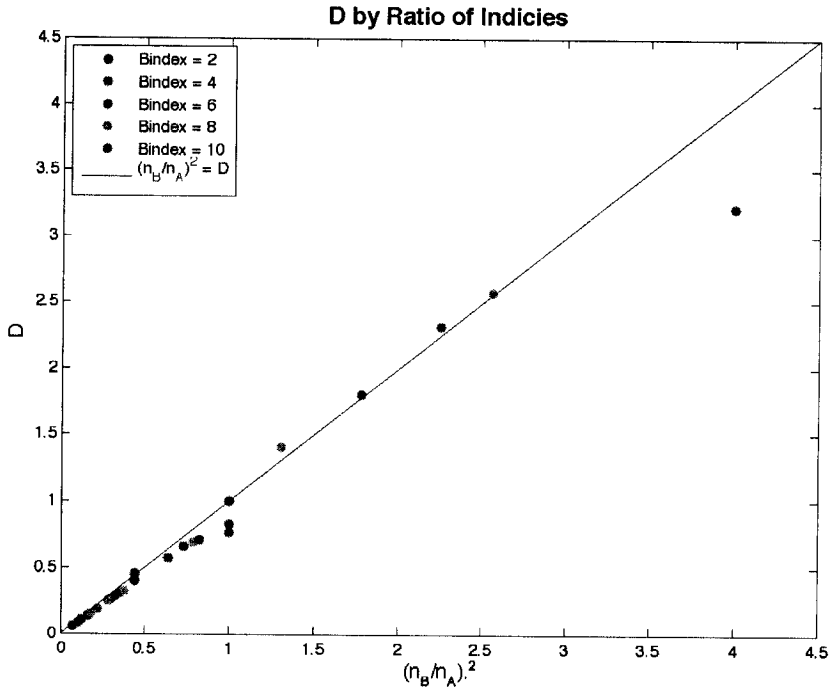

Figure 13: The relative error between the value of D as a function of the ratio of indices as predicted through linear theory.

between fixed points, is the same in both baroclinic and barotropic solitary waves and we can thus relate the indices, n_a and n_b, to the linear frequency. For a given oscillation period, T, the number of these nodes is such that

$$\begin{aligned} n_A &= T\omega_A = T\sqrt{\frac{b+1}{D}} \\ n_B &= T\omega_B = T. \end{aligned} \tag{7}$$

By noting T is the same in both A and B, we can then approximate the value of D for a given index by combining the two relationships above,

$$D \approx (b+1)(\frac{n_B}{n_A})^2. \tag{8}$$

For fixed $b = 0$, we plot the ratio of indices to the calculated value of the ratio of dispersions, D, and compare it to the theoretical value as predicted by linear theory in Figure (13). We find that the difference between our calculated value for D and

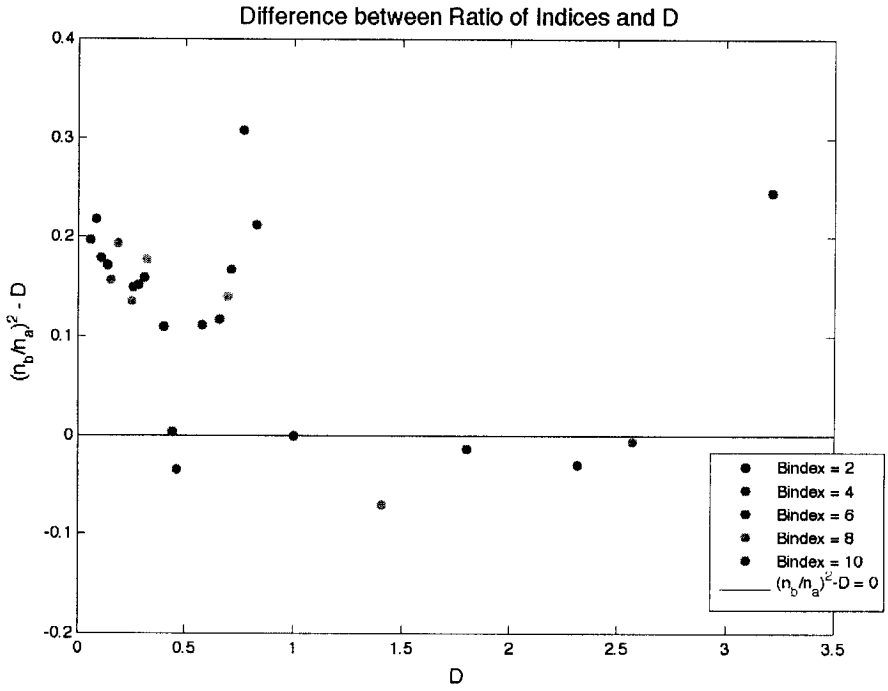

Figure 14: The difference between the value of D predicted by linear theory.

that predicted by our linear approximation is within 0.3 for most all identified indices (Figure 14). In general, the linear approximation is an underestimate for $D < 1$ and an overestimate for $D > 1$. Additionally, the linear approximation is best for small D, however it breaks down for vary large ratios of dispersion, such as the rogue point at $D = 3.2$ and in the limit as $D \to \infty$.

As the ratio of dispersions, D, becomes infinitely large, the orbit limits to the Eigenmode 1,2 heteroclinic solitary wave. This solitary wave cannot be found with the boundary value problem solver from Section 4.2, however we are able to show the cnoidal wave for large D using the initial value problem from Section 4.1 in Figure 15. The shape of the orbit, a near parabola in phase space, can be shown to limit to the curve $B = \frac{A^2}{2}$ by rescaling the traveling wave system, (2), and taking the limit as $D \to \infty$.

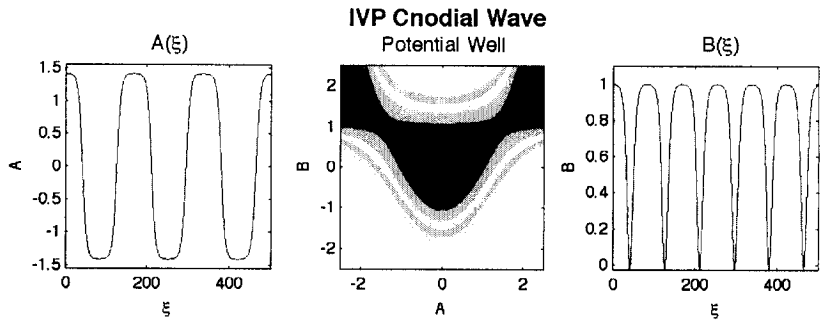

Figure 15: The Eigenmode 1,2 heteroclinic solitary wave in the limit as $D \to \infty$ as shown from the initial value problem. In this plot, we have chosen $D = 50$ and $A(0)$ and $B(0)$ within an ϵ distance of the right saddle point.

5 Atmospheric Solitary Waves

5.1 The Dimensional Wind Field

We now turn our attention to parameter regimes with physically relevant solitary wave solutions. In Section 4, we allowed for large, unrealistic variations in the ratio of dispersion of the baroclinic and barotropic Rossby wave field, D. For the boundary value problem in a fixed potential well, the ratio of dispersions ranged from 0.06 to 3.2, however none of these waves fall near the values of D calculated by Majda and Biello (2003), namely $D = 0.889$ and $D = 0.96$ for the first and second equatorial baroclinic modes, respectively. We now seek physically relevant, heteroclinic solitary wave solutions to (2) for a fixed D and a variable b and allow the size of the potential well to vary in a boundary value problem modified from the one used in Section 4.2 describing the coupled interaction of the first and second, $m = 1$ and 2, equatorial Rossby wave train with a barotropic Rossby wave train in a traveling reference frame.

Since Biello and Majda (2004) have already identified an analytic, homoclinic solitary wave solution to the MB equations, (1), we wish to focus on identifying heteroclinic solitary waves with realistic ratios of dispersions. Heteroclinic solitary waves represent a propagating disturbance in the wind field that reverses the climatology the tropical atmosphere in that the wind fields at the top and bottom of the troposphere to the west of the disturbance are flipped to the east of the disturbance and vice versa.

Mathematically, the change in background climatology in a traveling wave system is related to the fixed points of (2) and thus to the values of a and b. As we consider only a heteroclinic solitary wave, we force $a = 0$ and allow b to vary as the unknown eigenvalue in the boundary value problem solver. The fixed points in a symmetric potential well occur at $(\pm\sqrt{2(b+1)}, 1)$ in (A, B) phase space. In a heteroclinic orbit, the fixed points are the location of the asymptote in the baroclinic and barotropic wind fields as $\xi \to \pm\infty$.

We must re-dimensionalize the calculated values of A and B in order to consider the physical magnitude of the wind field. The values of A and B have been rescaled twice: once for $c = 1$ and once in Majda and Biello's (2003) development of the MB equations, (1). The dimensional values of these variables, indicated by a hat, are found in relation to the parameters used in this paper at a time $t = 0$ through

$$\hat{A} = \frac{A_0}{c}A, \ \hat{B} = \frac{B_0}{c}B, \ \hat{x} = x_0 c^{\frac{1}{2}}\xi \tag{9}$$

where the traveling wave speed, c, is undetermined. Majda and Biello (2003) show

the rescaling constants A_0, B_0, and x_0 are

$$(A_0, B_0, x_0) = \begin{cases} (0.613, 0.429, 0.60) & \text{for } m = 1 \\ (0.531, -0.377, 0.60) & \text{for } m = 2 \end{cases}$$

for the first and second, $m = 1$ and 2, baroclinic wave fields, respectively. For each m, Majda and Biello (2003) find a set ratio of dispersions, D, for in the interaction of the baroclinic and barotropic wave fields: $D = 0.889$ for $m = 1$ and $D = 0.96$ for $m = 2$. Through the linear theory discussed in Section 4.4, we expect to find the eigenmode 3,2 solitary wave at $b_1 = 1$ and $b_2 = 1.16$ for the $m = 1$ and 2 baroclinic regimes, respectively. For a fixed ratio of dispersions, D, we utilize a boundary value problem solver to find that $b_1 = 1.2$ and $b_2 = 1.4$, thus the linear approximation underestimates the value of the constant b for both the first and second baroclinic modes.

After finding b_1 and b_2 for the 3,2 heteroclinic solitary wave, we re-dimensionalize the baroclinic and barotropic wave amplitudes to obtain the physical wind field. At time $t = 0$, the barotropic wind field is governed by the stream function

$$\psi = -B(x)sin(ly) \tag{10}$$

where we have dropped the hats from the dimensional variables $\hat{B}$ and $\hat{x}$. For a given baroclinic mode, $l = \sqrt{2m+1}$.

The baroclinic wind field at time $t = 0$ is governed by (Heckley and Gill, 1984)

$$\begin{Bmatrix} p \\ u \\ v \end{Bmatrix} = \begin{Bmatrix} -\frac{A_m(x)}{\sqrt{2}}[D_{m-1} + \frac{D_{m+1}}{m+1}] \\ \frac{A_m(x)}{\sqrt{2}}[D_{m-1} - \frac{D_{m+1}}{m+1}] \\ -(\frac{2}{2m+1})A'_m(x)D_m \end{Bmatrix}$$

where $D_m = 2^{-\frac{m}{2}} H_m(y) e^{-\frac{y^2}{2}}$ are parabolic cylinder functions and A_m is the dimensional baroclinic wave field for a given meridional mode, m. The parabolic cylinder functions for $m = 1$ and 2 are functions themselves of the first four Hermite polynomials:

$$H_m(y) = \begin{cases} 1 & \text{for } m = 0 \\ 2y & \text{for } m = 1 \\ 4y^2 - 2 & \text{for } m = 2 \\ 8y^3 - 12y & \text{for } m = 3 \end{cases}$$

From our rescalings, (9), we note that the dimensional magnitude of the baroclinic and barotropic wind fields are proportional to c^{-1}. However, the scaled distance x is proportional to $c^{\frac{1}{2}}$. While the traveling wave speed is mathematically arbitrary, changing c changes the physical properties of the solitary wave. An increased traveling wave speed leads to an overall decrease in the maximum wind speeds, however it also stretches the zonal width of the disturbance wind field.

While we are able to set c to any positive value, thus producing an infinite number of solitary waves, we are restricted by the relevant physics of the traveling wave system. We choose an intermediate traveling wave speed, $c = 0.75$ to maintain wave amplitudes on the order of 5m/s while simultaneously satisfying the periodic boundary conditions in the zonal direction.

In order to satisfy periodic boundary conditions in x, all heteroclinic solitary waves must come in pairs. The length of the paired heteroclinic solitary waves are limited by the circumference of the Earth, approximately 40,000km. For the combined wind fields with $c = 0.75$, as shown in Figures 16 and 19, the zonal width of a single heteroclinic solitary wave disturbance field is approximately 20,000km, suggesting that a pair of these solitary waves would encircle the globe.

Additionally, these coupled Rossby waves travel at a modified wave speed, $V_{actual} = 1.5c - 16\text{m/s}$ where 16m/s is the wave speed of uncoupled Rossby waves. With our choice of $c = 0.75$, the heteroclinic solitary waves of Figures 16 and 19 travel at 14.875m/s westward.

The wind field for the first baroclinic mode and its corresponding barotropic mode at the bottom of the troposphere for $D = 0.889$ and $b_1 = 1.22$ are shown in Figure 17. Due to the antisymmetric baroclinic mode between the top and bottom of the troposphere, the combined wind profile at the top of the troposphere to the east of the disturbance is the same as the wind profile at the bottom of the troposphere to the west of the disturbance, as shown in Figure 16. Conversely, the barotropic wind field is zonally symmetric across the disturbance, as seen in Figure 17 and the wind fields at the bottom and top of the troposphere for the barotropic mode are the same.

The combination of these two wind fields, Figure 16, reveals an anticyclone pair centered at approximately $\pm$1000km off the equator that marks the boundary between weak equatorial easterlies to the west of the disturbance and strong equatorial westerlies to the east of the disturbance. To the west of the anticyclone pair are weaker midlatitude cyclonic circulations which can mainly be attributed to the barotropic mode as the baroclinic mode winds decay exponentially with increasing latitude.

While the first baroclinic wind field has an anticyclone pair at the equator, the combined wind field of the second baroclinic and barotropic modes for $D = 0.96$ and $b_2 = 1.4$ produces a more realistic equatorial climatology, since tropospheric background winds are observed to be easterlies, due to the change in sign of the dimensionality constant B_0 in the $m = 2$ meridional mode as shown in Figure (19). The second baroclinic wind field, in Figure 18, differs from the first baroclinic wind field mainly in the development of four zonal jets located off the equator as compared to the equatorially-centered three zonal jets in the $m = 1$ field. In Figure 18, these jets reverse direction across the disturbance. While these jets are

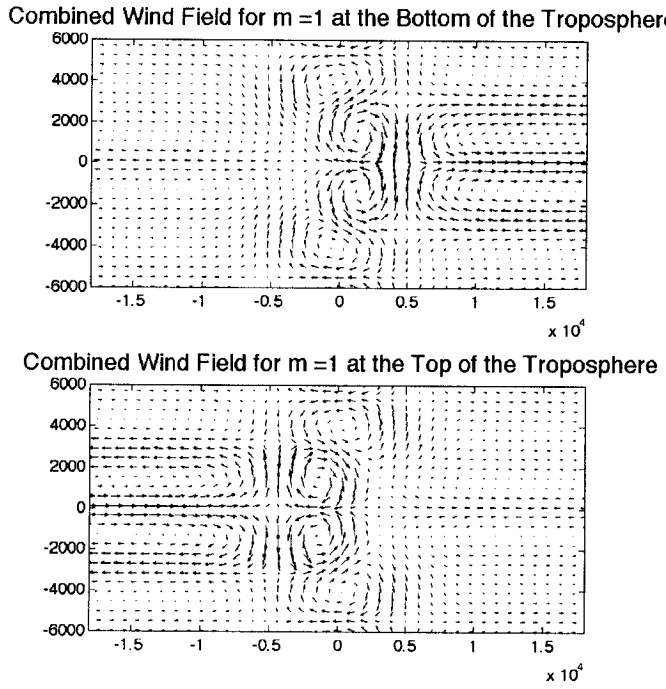

Figure 16: The combined baroclinic and barotropic wind fields in the upper and lower troposphere for the Eigenmode 3,2 heteroclinic solitary wave at with a meridional index $m = 1$ showing a reversal of the wind fields between the top and bottom of the troposphere.

still present in the combined wind field, Figure 19, the addition of the baroclinic wind field causes a meridional asymmetry in the magnitude of the wind field away from the solitary wave disturbance; to the west of the disturbance, the southern hemisphere westerly jet is stronger than the northern hemisphere easterly jet.

5.2 Discussion

The solitary wave solutions are a single, eastward propagating disturbance in both the baroclinic and barotropic wind fields which produce a long term, synoptic scale shift in the wind fields of the upper and lower troposphere. More importantly, these solitary waves represent a large-scale exchange of energy between the tropics and midlatitudes through the nonlinear interaction of equatorially confined baroclinic Rossby waves with barotropic Rossby waves with significant projection onto the midlatitudes.

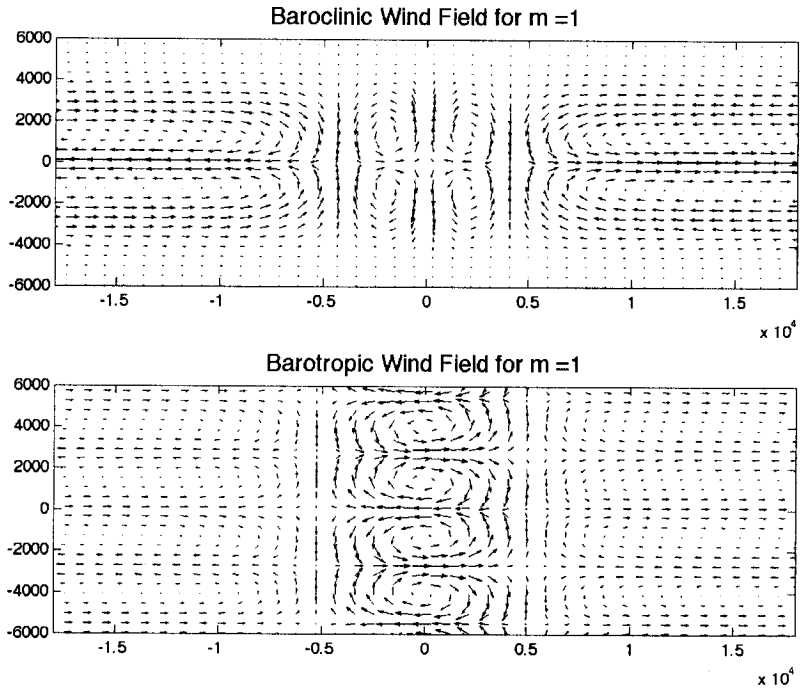

Figure 17: The baroclinc and barotropic wind fields for $m = 1$ for the Eigenmode 3,2 heteroclinic solitary wave at the bottom of the troposphere.

From the individual baroclinic and barotropic wind fields in Figures 17 and 18, we note that the structure of the solitary wave disturbance can mainly be attributed to the barotropic wind field. In the region of the disturbance, or within approximately 7500 km of the zero longitude line, the baroclinic wind field varies significantly in direction but is relatively weak in comparison to the strong cyclone-anticyclone pattern of the barotropic wind field.

At the bottom of the troposphere, the wind fields of both the first and second baroclinic modes have four weak centers of rotation, two cyclones and two anticyclones, however the first baroclinic mode has both cyclonic structures to the west of the $x = 0$ line while the second baroclinic mode has the cyclonic structures to the north-west and south-east of the origin. The stronger barotropic winds near the equator in the first (second) baroclinic modes lead to the dominant anticyclonic (cyclonic) centers in the combined wind field while the baroclinic winds shift the midlatitude cyclone (anticyclone) to the west (east) from the $x = 0$ line.

Unlike the winds around $x = 0$, the behavior of the combined wind field, Figures 16 and 19, outside of the region of disturbance can mainly be attributed to the

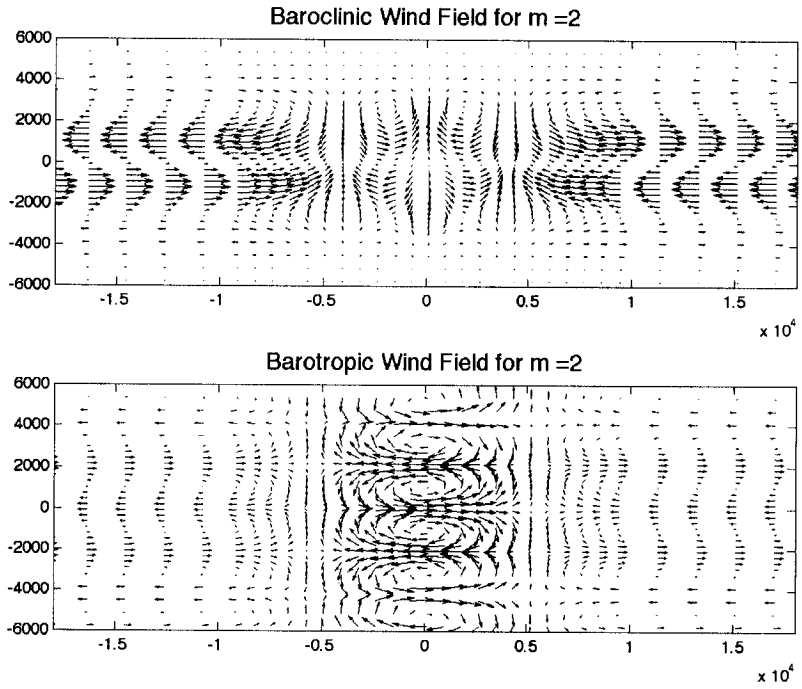

Figure 18: The baroclinc and barotropic wind fields for $m = 1$ for the Eigenmode 3,2 heteroclinic solitary wave.

baroclinic mode due to the comparatively strong zonal winds in these regions. We can attribute both the relative strength and direction of the background winds to the behavior of the solitary waves near the saddle fixed points. Away from the region of disturbance, or for large values of $|\xi|$ and likewise $|x|$, the magnitude of A' and B' go to zero as the solitary wave amplitude in the barotropic and baroclinic waves decay exponentially into the fixed points. Since the magnitude of the meridional component of the wind is proportional to A' and B', the winds become strictly zonal away of the disturbance region. Additionally, the location of the fixed point in the scaled baroclinic wave amplitudes, at $A = \pm\sqrt{2(b+1)}$, is always greater than that of the scaled barotropic wave amplitudes at $B = 1$ for $b > -\frac{1}{2}$ and, as a result, the magnitude of the wind away from the region of disturbance is greater in the baroclinic mode than in the barotropic mode.

While the disturbance wind fields are characterized by regions of strong cyclonic an anticyclonic rotation, the wind field away from the disturbance is characterized by zonal jets due to the lack of a meridional component to the wind field. As shown in Figure 16, the first baroclinic mode has two off-equator easterly jets

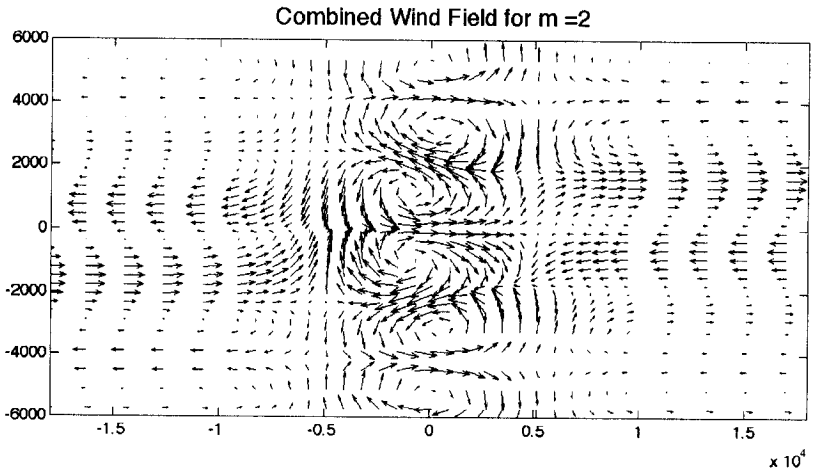

Figure 19: The combined baroclinic and barotropic wind fields for $m = 2$ for the Eigenmode 3,2 heteroclinic solitary wave.

located at approximately ±3500km north and south with a westerly jet centered on the equator. These jets are strong to the east of the disturbance field while the region west of the disturbance field is relatively quiet. The three jets in the first baroclinic mode are symmetric across the equator, unlike the four jets observed in the interaction of the second baroclinic Rossby wave with the barotropic Rossby wave, Figure 19, which are antisymmetric across the equator. The meridional symmetry of these jets are attributed to the Hermite polynomials of meridional mode, $m+1$, such that for $m = 1$ the zonal wind is approximately proportional to y^2, which is symmetric over $y = 0$. The zonal winds of the second baroclinic mode, however, are proportional to y^3 and are antisymmetric in y. The asymmetry in the zonal winds of the baroclinic mode, when combined with the symmetric barotropic winds, produces the off-equatorial, asymmetric jets in Figure 19.

While this model atmosphere has no explicit component of vertical velocity, we can estimate regions of possible rising and sinking motion by considering the convergence and divergence of the horizontal wind field. As discussed, the winds away from the disturbance field are primarily zonal and change little in x, thus

the only convergent regions of interest are located within the disturbance fields of Figures 16 and 19. In the interaction of the first baroclinic mode with the barotropic mode at the bottom of the troposphere, Figure 16, there is a region of strong meridional convergence and zonal divergence that is centered on the equator near the eastern edge of the anticyclone pair. To the west of the anticyclone pair, there is a region of exceptionally calm winds that is weakly divergent. Off the equator, we find regions of weak zonal convergence and meridional divergence at approximately 5000km east and 3800km north and south.

For the $m = 1$ combined wind field, none of these regions are regions of strong convergence or divergence, however for the $m = 2$ combined wind field, Figure 19, there is a clear region of convergence centered on the equator to the west of the cyclone pair. Such convergence at the bottom of the troposphere could suggest a region of rising motion and, although this model does not incorporate moisture in its dynamics, upward motion may be an indicator of possible convective activity.

The most significant interaction between the baroclinic and barotropic wind fields, however, does not lie in the zonal changes in the wind field but instead in the coupling between the midlatitudes and the tropics. From the combined wind fields of the first baroclinic mode, Figure 16, two tropical anticyclones are coupled to midlatitude cyclones while the combined wind fields of the second baroclinic mode, Figure 19, show a coupling between two tropical cyclones and two midlatitude anticyclones. This coupling occurs over a meridional distance of nearly 1,000km and suggests that midlatitude weather systems, whether cyclonic or anticyclonic, can couple with tropical systems through wave-wave interaction. In this idealized model, we see that a baroclinic mode, which may be driven by a localized heating in the tropics, can exchange energy with barotropic Rossby waves and thus with the midlatitudes, suggesting a meridional teleconnection between two different atmospheric regimes.

6 Acknowledgments

Research partially supported by an NSF VIGRE grant DMS 0636297 and by the Research Experience for Undergraduates (REU) program at the University of California, Davis. A. K. O'Rourke wishes to thank Prof. J. A. Biello for his guidance and support throughout this project.

7 Appendix

We have identified 28 solitary waves in the boundary value problem with $b = 0$ and three solitary waves for each of the $D = 0.889$ and $D = 0.96$ parameter

regimes. We include here a small selection of the solitary waves in order to show the diversity of solutions to the traveling wave system of equations, (2).

Figure 20 shows the first four fundamental heteroclinic solitary wave for the fixed-sized potential well with $b = 0$. We note the increasing trend in the ratios of dispersions, D, with increasing n_a and n_b indices. As viewed from left to right, each orbit circles the origin in a strictly clockwise manner and thus has a well-defined winding number. For Eigenmode 3,2, the solitary wave orbit makes one complete revolution around the origin and thus has a winding number of $n_\theta = 1$. For all fundamental solitary waves, we find that the winding number is directly related to the baroclinic wave index, n_a by $n_\theta = n_a - 1$.

Heteroclinic orbits that are not fundamentals are either overtones or have $D > 1$. Three of the first overtones are shown in Figure 21 and two of the second overtones are shown in Figure 22. Although heteroclinic orbits for $D > 1$ can have a well defined winding number, such as Eigenmode 3,4 in (a) of Figure 23, the ratio of dispersions is physically less than 1 from (3) and thus we do not consider these orbits as fundamentals.

In addition to the heteroclinic solitary waves focused on in this thesis, we also identified a number of homoclinic solitary waves in the boundary value problem from Section 4.2 with a fixed $b = 0$ for an unknown D. For $D < 1$, we show three of these homoclinic solitary waves in Figure 24 for $n_a = n_b$ while in Figure 25 we show two homoclinic solitary waves for $D > 1$.

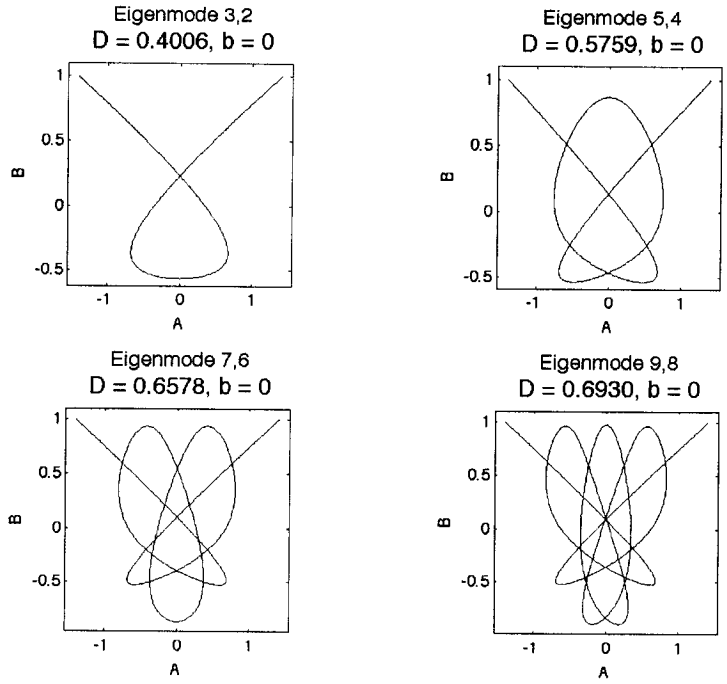

Figure 20: The first four fundamental heteroclinic solitary waves.

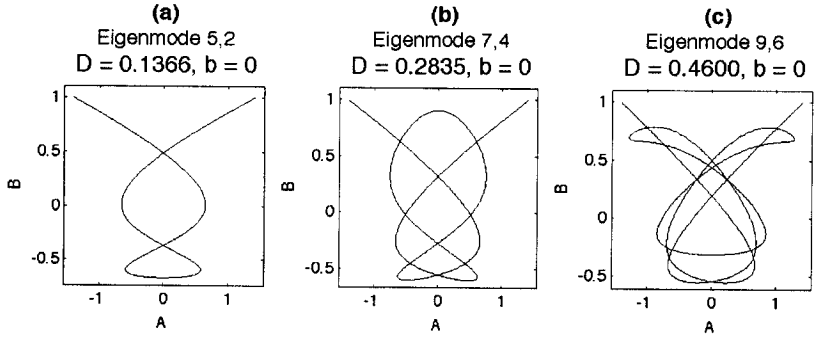

Figure 21: The first overtone for three heteroclinic solitary waves.

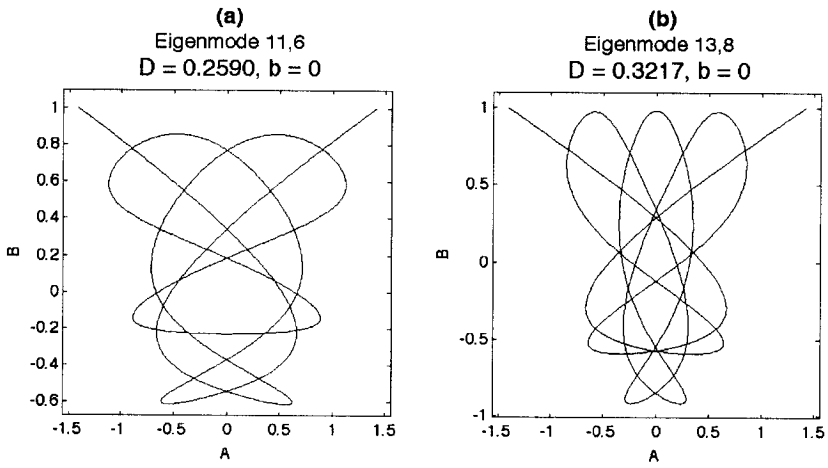

Figure 22: The second overtone for two heteroclinic solitary waves.

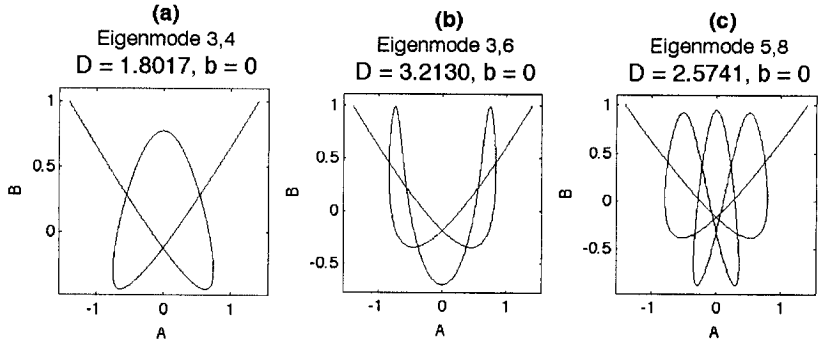

Figure 23: Three heteroclinic solitary waves with $D > 1$. Note the first curvature out of the fixed point is toward positive B.

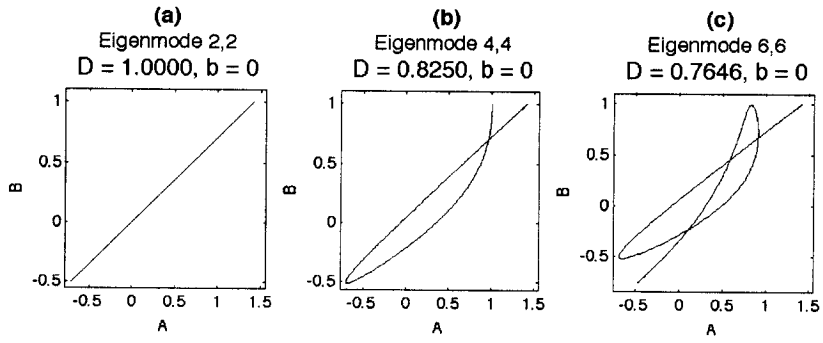

Figure 24: Homoclinic solitary waves with the same baroclinic and barotropic indices. Higher eigenmodes appear to extend the previous eigenmode's orbit in phase space.

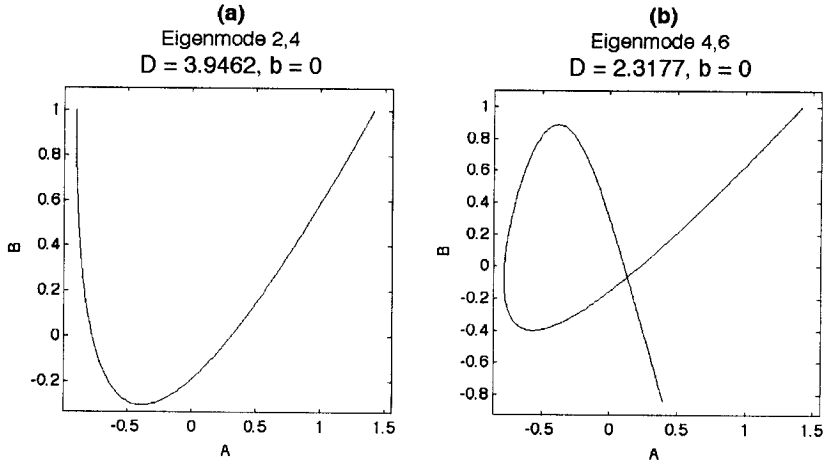

Figure 25: Two homoclinic solitary waves with $D > 1$.

References

[1] J. A Biello and A. J. Majda. The effect of meridional and vertical shear on the interaction of equatorial baroclinic and barotropic rossby waves. *Stud. Appl. Math.*, 112:341–390, 2004.

[2] W. A. Heckley and A. E. Gill. Some simple solutions to the problem of forced equatorial long waves. *Quart J. Roy. Metero. Soc.*, 110:203–217, 1984.

[3] A. Kasahara and P. L. Silva Dias. Response of lanetary waves to stationary tropical heating in a global atmosphere with meridional and vertical shear. *J. Atmos. Sci.*, 43:1893–1911, 1986.

[4] A. J. Majda and J. A. Biello. The nonlinear interaction of barotropic and equatorial baroclinic rossby waves. *J. Atmos. Sci.*, 60:1809–1821, August 2003.

[5] B. Wang and X. Xie. Low-frequency equatorial waves in vertically sheared zonal flow. part i: Stable waves. *J. Atmos. Sci.*, 53:449–467, 1996.

[6] P. J. Webster. Response of the tropical atmosphere to local steady forcing. *Mon. Wea. Rev.*, 100:518–541, 1972.